PHYSICAL REVIEW B **93**, 214303 (2016)

Phonon anharmonicity and components of the entropy in palladium and platinum

Yang Shen,[1,*] Chen W. Li,[1,2,3,†] Xiaoli Tang,[1] Hillary L. Smith,[1] and B. Fultz[1]

[1]*Department of Applied Physics and Materials Science, California Institute of Technology, Pasadena, California 91125, USA*

[2]*Geophysical Laboratory, Carnegie Institution for Science, Oak Ridge, Tennessee 37831, USA*

[3]*Spallation Neutron Source, Oak Ridge National Laboratory, Oak Ridge, Tennessee 37831, USA*

(Received 13 April 2016; published 6 June 2016)

Inelastic neutron scattering was used to measure the phonon density of states in fcc palladium and platinum metal at temperatures from 7 K to 1576 K. Both phonon-phonon interactions and electron-phonon interactions were calculated by methods based on density functional theory (DFT) and were consistent with the measured shifts and broadenings of phonons with temperature. Unlike the longitudinal modes, the characteristic transverse modes had a nonlinear dependence on temperature owing to the requirement for a population of thermal phonons for upscattering. Kohn anomalies were observed in the measurements at low temperature and were reproduced by calculations based on DFT. Contributions to the entropy from phonons and electrons were assessed and summed to obtain excellent agreement with prior calorimetric data. The entropy from thermal expansion is positive for both phonons and electrons but larger for phonons. The anharmonic phonon entropy is negative in Pt, but in Pd it changes from positive to negative with increasing temperature. Owing to the position of the Fermi level on the electronic DOS, the electronic entropy was sensitive to the adiabatic electron-phonon interaction in both Pd and Pt. The adiabatic EPI depended strongly on thermal atom displacements.

DOI: 10.1103/PhysRevB.93.214303

I. INTRODUCTION

Phonon scattering has long been a subject of interest for transport properties and thermodynamics of solids. In insulators, phonon-phonon scattering is the dominant mechanism, but electron-phonon scattering is also important for metals [1–3]. The interplay between the scattering of phonons and electrons originates with the basic electronic and phonon structures of a metal but leads to thermodynamic behavior that is challenging to understand. In previous studies of nearly-free electron metals with low electron densities of states near the Fermi level [4–6], electron-phonon interactions were weak, so phonon-phonon interactions were primarily responsible for the lifetime broadening of phonon energies. Transition metals, with their much higher densities of states near the Fermi level, generally have stronger electron-phonon interactions at low temperatures [7–11], giving these metals and alloys high critical temperatures for conventional superconductivity, for example. Electron-phonon interactions persist well above the superconducting transition temperature, however, and their effects on high temperature thermodynamics can be significant [12–14]. Phonon-phonon interactions increase with more thermal phonons, and the effects of temperature on thermodynamics can involve a number of competing mechanisms beyond the harmonic or quasiharmonic approximations of phonon behavior [15].

Effects of phonon-phonon scattering can be observed by inelastic neutron scattering experiments. These anharmonic effects cause shifts and broadenings of the measured phonon spectra [2,3,16,17]. Unfortunately, it is usually not possible to decouple the effects of phonon-phonon interactions from effects of electron phonon using measurements alone [3]. First-principles calculations of the scattering rate of each mechanism are useful for identifying the dominant scattering mechanism and for better understanding the materials physics at the atomic level.

Palladium and platinum have commercial and technological importance for chemical engineering, electronics, dentistry, medicine, and fashion [18–20]. Their thermal physics is interesting to compare because they lie in the same column of the periodic table, with similar electronic and phonon band structures. Both have strong electron-phonon interactions owing to their high densities of electronic states at the Fermi level. A previous first-principles study [21] of electron-phonon interactions in Pd gave phonon linewidths comparable to the measured linewidth at 4.5 K, indicating that electron-phonon interactions dominate the linewidth. However, a parallel calculation for Pt is not yet available. Furthermore, the temperature dependences of electron-phonon and phonon-phonon interactions have received little study.

Here we report results from a combined experimental and theoretical study on the phonon dynamics of face-centered-cubic Pd and Pt metals. Inelastic neutron scattering experiments were performed to measure the phonon density of states of Pd and Pt at temperatures from 7 K to 1576 K. The contributions of electron-phonon and phonon-phonon scattering to the phonon linewidths were calculated by perturbation theory using methods based on density functional theory (DFT). We present the measured phonon density of states of Pd and Pt at several temperatures, then show the calculated phonon linewidths from both electron-phonon and phonon-phonon interactions and their variations with temperature. We find slightly stronger electron-phonon interactions in Pd than Pt, but slightly stronger phonon-phonon interactions in Pt. With some care to define the different contributions to the entropy [2], we report the temperature dependences of the entropic contributions from thermal expansion, phonon anharmonicity, and the adiabatic electron-phonon interaction.

---

[*] yshen@caltech.edu

[†] chenwli@gmail.com

The sum of all contributions is compared with the entropy from calorimetric measurements, with excellent results.

II. EXPERIMENT

Platinum and palladium metals of 99.9% or higher purity were formed into plates with thicknesses of 0.82 and 2.25 mm, respectively, giving ratios of multiply- to singly-scattered neutrons of 9.0% and 9.6%. Neutron inelastic scattering measurements were performed with the time-of-flight Fermi chopper spectrometer, ARCS, at the Spallation Neutron Source at Oak Ridge National Laboratory. The incident neutron energy was 50.0 meV, and each measurement included a total of approximately 6.0 C proton charge on the spallation target. For temperatures of 7 and 300 K, the sample was mounted in a closed-cycle helium refrigerator. For temperatures of 326, 576, 876, 976, 1176, 1376, and 1576 K, the sample was mounted in a high temperature, electrical resistance furnace (MICAS furnace) designed for vacuum operation in the ARCS spectrometer.

Data reduction was performed with a standard software package for the ARCS instrument [22]. The raw data of individual neutron detection events were first binned to get $I(E,2\theta)$, where 2θ is the scattering angle and E is the energy transfer, and normalized by the proton current on target. Bad detector pixels were identified and masked, and the data were corrected for detector efficiency using a measurement from vanadium. The $I(E,2\theta)$ were then rebinned into intensity, $I(Q,E)$, where $\hbar Q$ is the momentum transfer to the sample. The E ranged from –49.75 to 50.25 meV, with a bin width of 0.5 meV. The elastic peak was removed below 3.0 meV and replaced by a function of energy determined from the inelastic scattering just past the elastic peak [23]. The phonon DOS curves were obtained after corrections for multiphonon and multiple scattering, as described previously [23]. The averaging over all Q for a given E will eliminate effects of coherent interference between single- and two-phonon scattering.

III. COMPUTATIONAL METHODOLOGY

The contribution to the phonon linewidth from phonon-phonon scattering ($2\Gamma_{\text{ph-ph}}$) is [16,17]

$$
\begin{aligned}
2\Gamma_{\text{ph-ph}}(\mathbf{q},j) = {}& \frac{\pi\hbar}{8N} \sum_{\mathbf{q}_1,\mathbf{q}_2,j_1,j_2} \Delta(\mathbf{q}_1+\mathbf{q}_2-\mathbf{q}) \\
& \times \frac{|\Phi(-\mathbf{q}j;\mathbf{q}_1 j_1;\mathbf{q}_2 j_2)|^2}{\omega(\mathbf{q}j)\omega(\mathbf{q}_1 j_1)\omega(\mathbf{q}_2 j_2)} [(n_1+n_2+1) \\
& \times \delta(\omega-\omega_1-\omega_2) + 2(n_1-n_2)\delta(\omega+\omega_1-\omega_2)],
\end{aligned}
\tag{1}
$$

where N is the number of unit cells, $\hbar$ is the Planck constant over 2π, and n is the Planck distribution function. Here Φ is the phonon-phonon coupling matrix element for a three-phonon process.

The contribution to the phonon linewidth from electron-phonon scattering ($2\Gamma_{\text{e-ph}}$) is

$$
\begin{aligned}
2\Gamma_{\text{e-ph}}(\mathbf{q},j) = {}& 2\pi\omega_{\mathbf{q},j} \sum_{\mathbf{k},\text{i},\text{f}} |g(\mathbf{k}_\text{i},\mathbf{k}_\text{f},\mathbf{q},j)|^2 \\
& \times \delta(E_{\mathbf{k}_\text{i}} - E_F)\delta(E_{\mathbf{k}_\text{f}} - E_F)\ ,
\end{aligned}
\tag{2}
$$

where $\omega_{\mathbf{q},j}$ is the phonon frequency. The $g(\mathbf{k}_\text{i},\mathbf{k}_\text{f},\mathbf{q},j)$ is the electron-phonon matrix element, where the phonon $(\mathbf{q},j)$ scatters an electron from the initial state $\mathbf{k}_\text{i}$ with energy $E_{\mathbf{k}_\text{i}}$ to the final state $\mathbf{k}_\text{f}$ with energy $E_{\mathbf{k}_\text{f}}$.

All calculations were performed in the local density approximation with pseudopotentials and a plane-wave basis set. The phonon-phonon coupling matrix Φ of Eq. (1) was calculated using the small-displacement supercell method with forces from density functional theory implemented in VASP code [24–26]. Details of implementation can be found in our previous study [6]. This real-space method used 256-atom supercells, with both positive and negative displacements of 0.02 Å to cancel effects from higher-order anharmonicities. Phonon linewidths were calculated with Eqn. 1 using a q-point grid of 24 × 24 × 24 for the Brillouin zone integration.

For the electron-phonon linewidth $2\Gamma_{\text{e-ph}}$ at 0 K, the electron-phonon matrix element $g(\mathbf{k}_\text{i},\mathbf{k}_\text{f},\mathbf{q},j)$ was calculated using density functional perturbation theory as implemented in the QUANTUM-ESPRESSO package [27]. The first-order Hermite Gaussian smearing technique with a width of 0.022 Ryd was used to account for the presence of a Fermi surface. A k-space sampling grid of 24 × 24 × 24 was used for the Brillouin zone integration of Eq. (2). Since both $2\Gamma_{\text{ph-ph}}$ and $2\Gamma_{\text{e-ph}}$ are calculated with respect to the phonon energy itself, the inconsistency of using two different *ab initio* computing engines is minimized by choosing the PAW-LDA pseudopotentials that yield comparable phonon and electron band structures.

IV. RESULTS AND DISCUSSION

A. Phonon dispersions and DOS, Kohn anomalies

Figures 1(a) and 1(b) show the calculated phonon dispersions along high symmetry directions at 0 K, along with previous inelastic neutron scattering measurements at 296 K for Pd [28] and 90 K for Pt [29]. The agreement is excellent. The dispersion curves of Pd and Pt have similar features, but the energies are shifted upwards for Pd compared to Pt. The shifts are about 50 to 65% of what is expected from the mass difference alone, indicative of stronger interatomic forces in Pt. This is also seen in Figs. 2(a) and 2(b) that show the phonon densities of states (DOS) of Pd and Pt measured in this work at temperatures from 7 K to 1576 K. With increasing temperature, features of the DOS shift downwards in energy (soften) and the features broaden in energy.

Kohn anomalies were previously reported in the phonon dispersions of both Pd and Pt along the [011] direction [28–30]. They are also reproduced by our calculations at $\mathbf{q}_{\text{cal}} \simeq \frac{2\pi}{a}[0.31,0.31,0]$, slightly lower than the experimental result of $\mathbf{q}_{\text{exp}} \simeq \frac{2\pi}{a}[0.35,0.35,0]$. Effects of Kohn anomalies are also seen around 8 meV in our experimental phonon DOS for both Pd and Pt at 7 K (Fig. 2). These features are diminished with temperature, and are no longer visible at temperatures around 900 K or so.

B. Measured phonon shifts and broadenings

Temperature causes the peaks in the experimental phonon DOS of both Pd and Pt to broaden, and shift to lower energy (Fig. 2). The thermal softening of phonons in Pd is more rapid

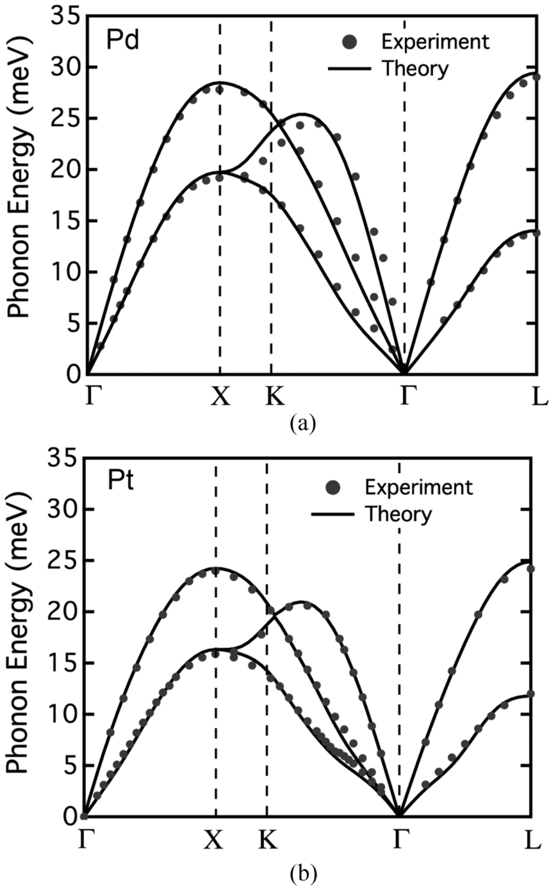

(a)

(b)

FIG. 1. Calculated phonon dispersions of (a) Pd and (b) Pt along high symmetry directions, with points from experimental data of Refs. [28,29].

than in Pt. This may reflect the stiffer interatomic forces in Pt. The thermal shift was approximated by rescaling all energies with a constant mutiplier, η,

$$E' \longmapsto \eta E'. \tag{3}$$

The thermal broadening, which was more prominent than the thermal shift, was modeled with the spectral weight function of a damped harmonic oscillator [31], centered about energy E' with the quality factor $\mathcal{Q}$. The broadening function $B(\mathcal{Q};E,E')$ is

$$B(\mathcal{Q};E,E') = \frac{1}{\pi \mathcal{Q} E'} \frac{1}{\left(\frac{E'}{E} - \frac{E}{E'}\right)^2 + \frac{1}{\mathcal{Q}^2}}. \tag{4}$$

Using Eqs. 3 and 4, the measured phonon DOS at temperature T, $g_T(E)$, was fit to an convolutionlike integral transform of $g_{7\mathrm{K}(E)}$, the rescaled phonon DOS measured at the lowest temperature of 7 K

$$\begin{aligned} g_T(E) &= \int B(\mathcal{Q};E,E') g_{7\mathrm{K}}(\eta E') dE' \\ &\triangleq B(\mathcal{Q};E,E') \odot g_{7\mathrm{K}}(\eta E') . \end{aligned} \tag{5}$$

In principle, each phonon mode has a unique thermal shift and broadening, but it has proved useful and more practical to work with averaged values of η and $\mathcal{Q}$ for the full phonon DOS, as was previously reported for Al [23]. This approach is demonstrated in Fig. 3(a), and it is evident that the calculated broadening is too large for the low-energy peak of the DOS, and the broadening is too small for the high-energy peak. The high quality of our experimental phonon DOS for Pd and

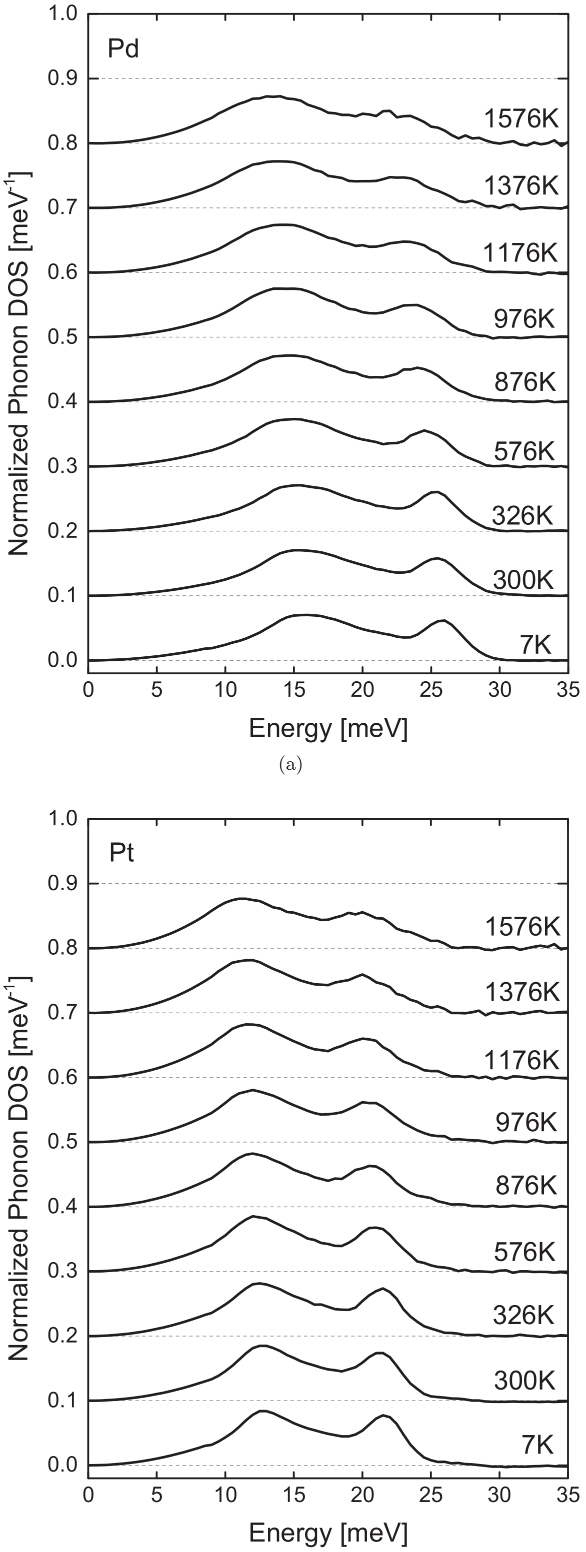

(a)

(b)

FIG. 2. Experimental phonon DOS curves of Pd (a) and Pt (b) normalized to unity. Curves are offset for clarity.

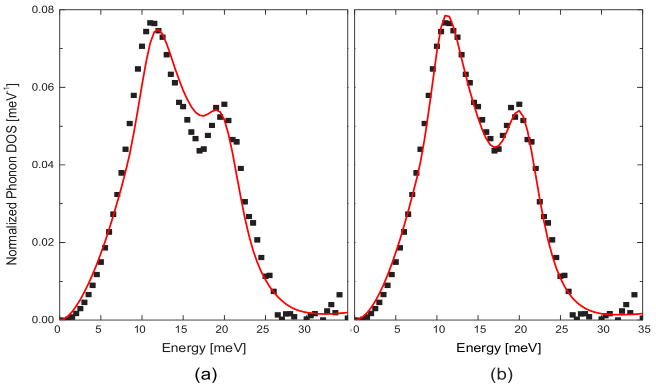

FIG. 3. Fittings of Pt phonon DOS at 1576 K using broadened, shifted DOS curve from 7 K. (a) Fit using Eq. 5. (b) Fit using Eq. 6 with separate transverse and longitudinal components.

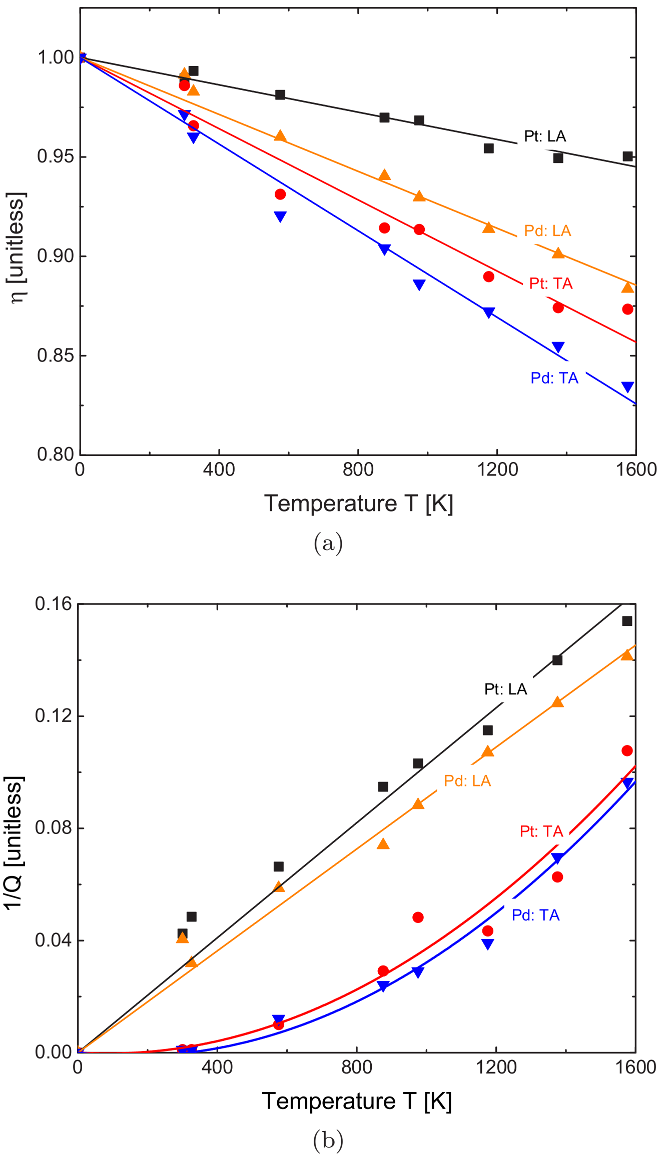

(a)

(b)

FIG. 4. Temperature dependences from data of Fig. 2 for (a) phonon shift η vs. T, and (b) broadening $1/\mathcal{Q}$ vs. T for Pd and Pt.

Pt made it practical to fit separately the two main features of the DOS, which originate primarily from transverse and longitudinal modes, by rewriting Eq. (5) as

$$g_T(E) = B(\mathcal{Q}^{\mathrm{TA}}; E,E') \odot g^{\mathrm{TA}}_{7\,\mathrm{K}}(\eta^{\mathrm{TA}}E') + B(\mathcal{Q}^{\mathrm{LA}}; E,E') \odot g^{\mathrm{LA}}_{7\,\mathrm{K}}(\eta^{\mathrm{LA}}E'). \qquad (6)$$

The $g^{\mathrm{TA}}_{7\,\mathrm{K}}$ and $g^{\mathrm{LA}}_{7\,\mathrm{K}}$ were obtained by fitting the two features of the DOS curve at 7 K to Lorentzian functions. For each temperature, the four factors $\{\mathcal{Q}^{\mathrm{TA}}, \eta^{\mathrm{TA}}; \mathcal{Q}^{\mathrm{LA}}, \eta^{\mathrm{LA}}\}$ were determined through a least-squares algorithm implemented with gradient descent. A resulting fit is shown in Fig. 3(b), giving better agreement than when the transverse and longitudinal features are not differentiated as in Fig. 3(a).

Figures 4(a) and 4(b) show the temperature dependence of the shift and broadening parameters $\{\mathcal{Q}^{\mathrm{TA}}, \eta^{\mathrm{TA}}; \mathcal{Q}^{\mathrm{LA}}, \eta^{\mathrm{LA}}\}$. The transverse modes soften faster with temperature than the longitudinal modes in both Pt and Pd, but all are linear with temperature. An approximately linear temperature dependence is also seen for the broadening of the longitudinal modes as shown in Fig. 4(b) for $1/\mathcal{Q}$ vs. T. However, the thermal broadening of the transverse modes is distinctly nonlinear, at least for temperatures below 1000 K.

C. Electron-phonon and phonon-phonon interactions, phonon linewidths

Figures 5 and 6 present $2\Gamma_{\text{e-ph}}$ and $2\Gamma_{\text{ph-ph}}$ for phonons along high symmetry directions for both Pd and Pt at 0 K. The phonon linewidths of Pd are in the range of 0 to 0.3 meV, similar to those of a previous study [21], and comparable to experimental measurements [30]. We found that $2\Gamma_{e-p}$ is comparable for Pd and Pt.

The overall electron-phonon coupling strength can be described by a dimensionless parameter [32]

$$\lambda = \sum_{\mathbf{q},j}\lambda_{\mathbf{q},j} = \sum_{\mathbf{q},j}\frac{\Gamma_{\mathbf{q},j}}{\pi N_{\mathrm{F}}\omega^2_{\mathbf{q},j}}\,, \qquad (7)$$

where N_{F} is the electron density of states at the Fermi energy, and $\omega_{\mathbf{q},j}$ and $\Gamma_{\mathbf{q},j}$ are the phonon angular frequency and linewidth. The Fermi surface was broadened in energy with Gaussian functions as implemented in the QUANTUM-ESPRESSOpackage [27], so electron-phonon coupling strengths λ were calculated as a function of broadening, σ. The converged value of λ was obtained at $\sigma = 0.25$ Ryd, which is the minimal possible broadening that still achieves convergence [32]. Our calculated values of λ are 0.41 and 0.59 for Pd and Pt respectively, which are close to the empirical values [33] of 0.47 and 0.66.

Figure 6 shows $2\Gamma_{\text{ph-ph}}$ at 0 K, which is similar for both Pd and Pt. At 0 K the TA modes are an order-of-magnitude narrower than the higher energy LA modes. Comparing Fig. 5 with Fig. 6, the $2\Gamma_{\text{e-ph}}$ and $2\Gamma_{\text{ph-ph}}$ are comparable for LA modes, but the $2\Gamma_{\text{e-ph}}$ are much larger than the $2\Gamma_{\text{ph-ph}}$ for TA modes. At 0 K, LA phonons are effectively scattered by both electrons and other phonons, whereas TA phonons are scattered mostly by electrons. Figure 7 shows the phonon linewidths at 900 K. Here the $2\Gamma_{\text{ph-ph}}$ at 900 K are nearly

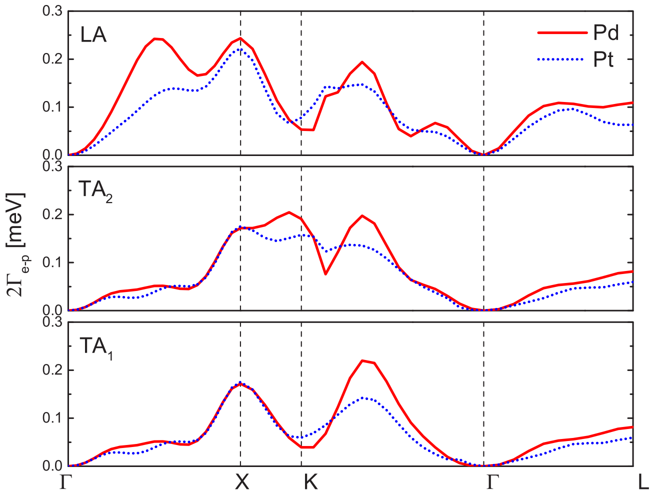

FIG. 5. Electron-phonon contributions to phonon linewidth of Pd (solid line) and Pt (dotted line) at 0 K.

10 times larger than $2\Gamma_{\text{e-ph}}$ at 0 K, showing the dominance of phonon-phonon interactions at high temperatures.

The trends of Fig. 4(b) are supported by Figs. 6 and 7. At low temperatures only down-conversion processes are possible, and there are more down-scattering channels for LA than TA modes. The broadening of transverse modes by up-scattering involves the annihilation of phonons, and does not occur unless enough thermal phonons are available. Figure 4 shows that the thermal broadenings of phonons in Pd and Pt are very similar, however, consistent with experimental results from Sec. IV B. At higher temperatures, three-phonon processes dominate the broadening. These are quite similar for Pd and Pt, consistent with their rather similar phonon dispersions shown in Fig. 1. Approximately, at 900 K the broadening of the longitudinal feature of the Pd phonon DOS has a breadth of $1/Q = 0.09$ from Fig. 4(b), and an energy of 24 meV from Fig. 2, giving a broadening of 2.2 meV. This is in agreement with the broadenings calculated from phonon-phonon interactions shown in Fig. 7. The phonon lifetime broadenings may cause an analysis of the measured phonon DOS to underestimate the vibrational entropy by 0.1 k_B/atom at 1600 K [31], but we did not correct the vibrational entropy for this small effect in what follows.

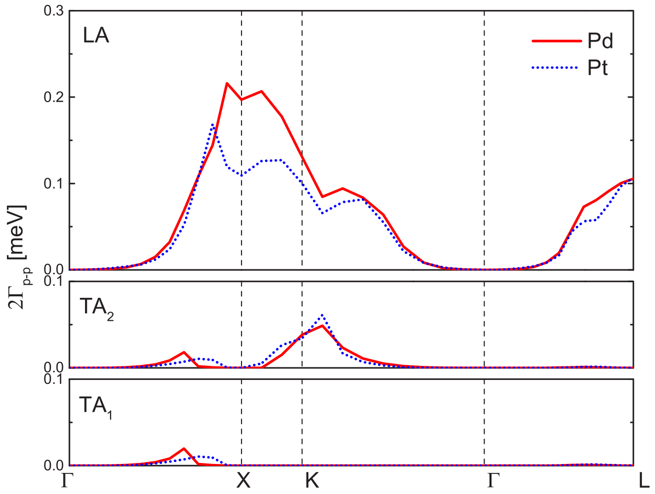

FIG. 6. Phonon-phonon contributions to phonon linewidth of Pd (solid line) and Pt (dotted line) at 0 K.

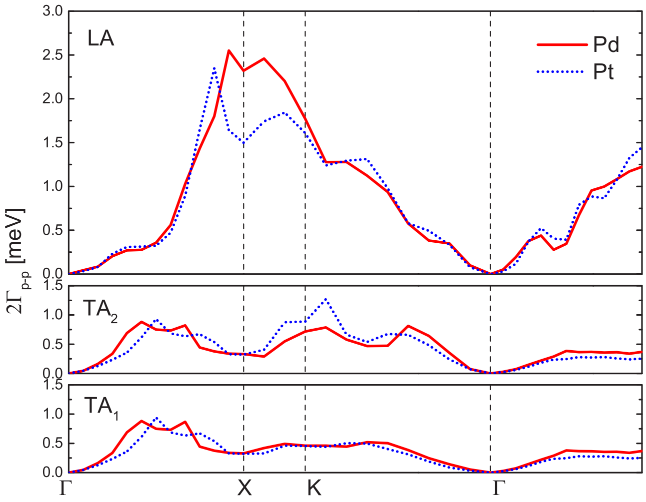

FIG. 7. Phonon-phonon contributions to phonon linewidth of Pd (solid line) and Pt (dotted line) at 900 K.

D. Entropy

For Pd and Pt, the contributions to the entropy [34] are from phonons (S_{ph}), electrons (S_{el}), their interactions (S_{ep}), and the lattice configurations (S_{cf})

$$S_{\text{tot}} = S_{\text{ph}} + S_{\text{el}} + S_{\text{ep}} + S_{\text{cf}} \;. \tag{8}$$

The entropy from the nonadiabatic electron-phonon interaction, $S_{\text{ep}}^{\text{na}}$, is from the mixing of the electron ground states from the nuclear motion. It dominates at low temperatures [2], but the adiabatic electron-phonon entropy $S_{\text{ep}}^{\text{ad}}$ is larger at higher temperatures. This $S_{\text{ep}}^{\text{ad}}$ accounts for the thermal shifts of electron states caused by average nuclear motions [2]. The total entropy is now

$$S_{\text{tot}} = S_{\text{ph}} + S_{\text{el}} + S_{\text{ep}}^{\text{na}} + S_{\text{ep}}^{\text{ad}} + S_{\text{cf}} \;. \tag{9}$$

We obtained the total phonon entropy from the experimental phonon DOS shown in Fig. 2 using the expression

$$S_{\text{ph}}(T) = 3k_{\text{B}} \int \mathrm{d}E \; g_T(E) \times [(n_T + 1)\ln(n_T + 1) - n_T \ln(n_T)], \tag{10}$$

where $g_T(E)$ is the phonon DOS and $n_T(E)$ is the Planck distribution, both at the temperature of interest, T. When $g_T(E)$ is measured at the temperature of interest, Eq. 10 is rigorously correct for the effect of harmonic and quasiharmonic vibrations on the entropy, and for the effects of electron-phonon interactions on these vibrations. It also provides a good accounting for the anharmonic shifts of vibrational frequencies [3,15,34].

For identifying the different types of nonharmonic behavior, an ideal harmonic crystal is a convenient reference. The harmonic entropy $S_{\text{ph,H}}$ is obtained by assuming the low-temperature phonon DOS is unaltered by temperature, so to obtain $S_{\text{ph,H}}$ we used the DOS measured at 7 K in Eq. 10, with the Planck occupancy $n_T(E)$ for the (higher) temperatures of interest.

Thermal expansion gives the quasiharmonic contribution to the phonon entropy, $\Delta S_{\text{ph,QH}}$

$$\Delta S_{\text{ph,QH}}(T) = 9\int_0^T B v \alpha^2 \mathrm{d}T', \tag{11}$$

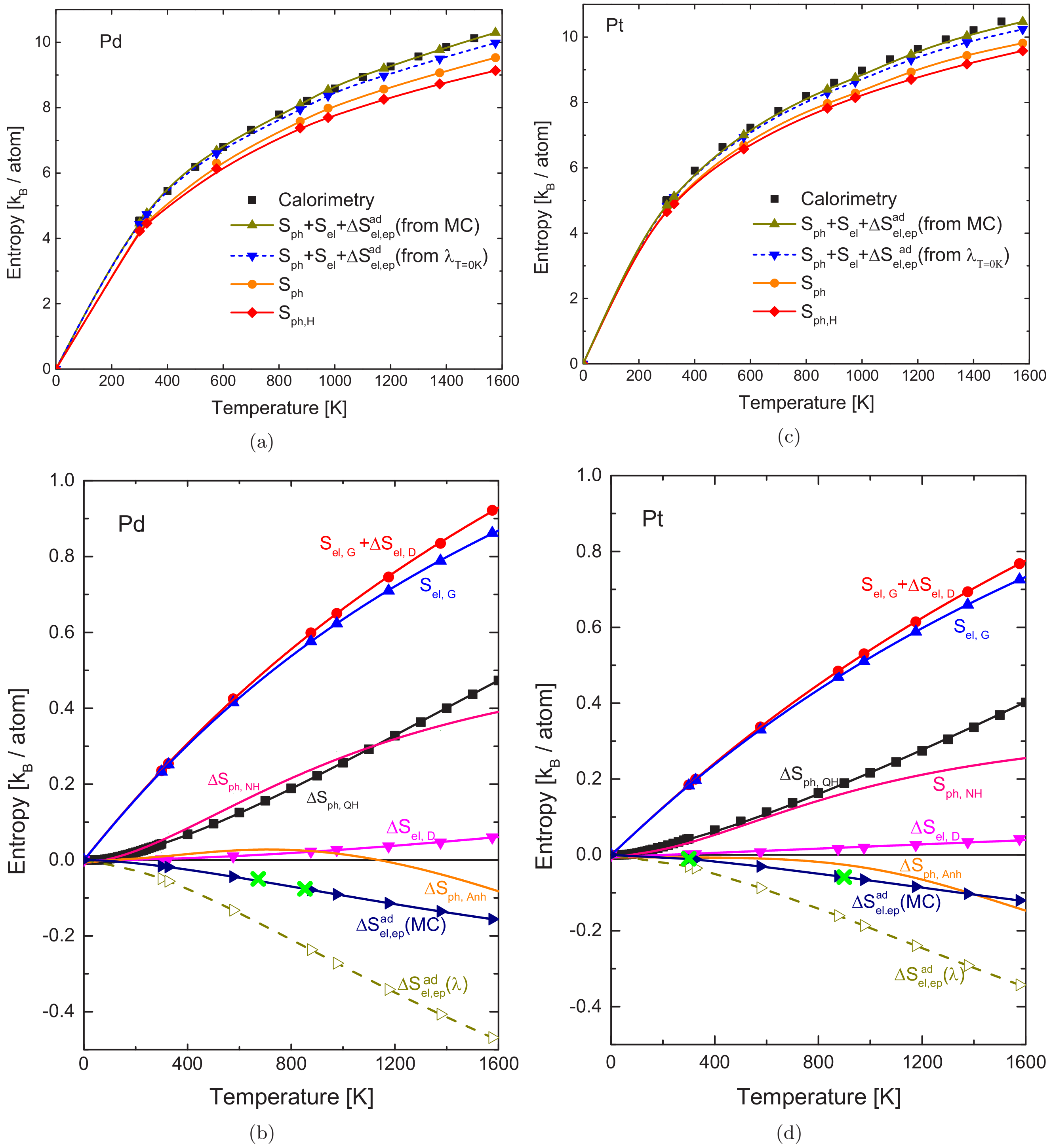

(a) (c)

(b) (d)

FIG. 8. The origins of entropy of (a),(b) Pd and (c),(d) Pt. (a),(c) “Calorimetry” points are from Arblaster [44,45], S_{ph} are from data of Fig. 2 and Eq. (10), $S_{\text{ph,H}}$ was calculated with Eq. (10) and the measured phonon DOS at 7 K, and S_{el} is the sum of $S_{\text{el,G}}$ and $\Delta S_{\text{el,D}}$. (b),(d) The different minor contributions less than 10% of the total entropy. They are from the lattice dilation influence on phonons and electrons ($\Delta S_{\text{ph,QH}}$, $\Delta S_{\text{el,D}}$), the anharmonicity ($\Delta S_{\text{ph,Anh}}$), and the adiabatic EPI induced thermal broadening in electron DOS ($\Delta S^{\text{ad}}_{\text{el,ep}}$). The $\Delta S^{\text{ad}}_{\text{el,ep}}$ was first calculated using the electron-phonon coupling parameter, λ at $T = 0$ K ($\Delta S^{\text{ad}}_{\text{el,ep}}(\lambda)$), and then rescaled by Monte Carlo calculations to give our preferred $\Delta S^{\text{ad}}_{\text{el,ep}}$(MC).

where B is the isothermal bulk modulus, obtained from the literature [35–39], v is the specific volume [40,41] and α is the linear coefficient of thermal expansion [40,41], and all must be taken at the temperature T'. [2] The anharmonic contribution to the phonon entropy ($\Delta S_{\mathrm{ph,Anh}}$) and the nonharmonic contribution ($\Delta S_{\mathrm{ph,NH}}$) are

$$\Delta S_{\mathrm{ph,Anh}} = S_{\mathrm{ph}} - S_{\mathrm{ph,H}} - \Delta S_{\mathrm{ph,QH}} \tag{12}$$

$$\Delta S_{\mathrm{ph,NH}} = S_{\mathrm{ph}} - S_{\mathrm{ph,H}} \tag{13}$$

$$\Delta S_{\mathrm{ph,NH}} = \Delta S_{\mathrm{ph,QH}} + \Delta S_{\mathrm{ph,Anh}}. \tag{14}$$

As fermions, the entropy from the electrons is

$$S_{\mathrm{el}}(T) = -k_{\mathrm{B}} \int \mathrm{d}E\; N_T(E) \times [(1 - f_T)\ln(1 - f_T) + f_T \ln(f_T)], \tag{15}$$

where $N_T(E)$ is the electronic DOS and $f_T(E)$ is the Fermi distribution function, both at the temperature of interest, T. To separate the effect of thermal expansion, we define the "ground state" electronic entropy, $S_{\mathrm{el,G}}(T)$ by using the electronic DOS at $T_0 = 0\mathrm{K}$, $N_{\mathrm{G}}(E)$, but using the Fermi distribution at temperature T in Eq. 15. Taking dilation into account, the electronic DOS, $N_D(E)$, was calculated for volumes consistent with thermal expansion. The dilation effect is separated from the ground state electronic entropy as

$$\Delta S_{\mathrm{el,D}} = S_{\mathrm{el}}(N_{\mathrm{D}}) - S_{\mathrm{el}}(N_{\mathrm{G}}). \tag{16}$$

Once $\Delta S_{\mathrm{el,D}}$ is calculated at a low-temperature volume and a high-temperature volume, an interpolation can be performed for intermediate temperatures [42].

The adiabatic electron-phonon interaction (EPI) causes a thermal broadening of electron levels. Following Thiessen [43], we used an electronic broadening function of Lorentzian form with full-width-at-half-maximum $2\Gamma = 2\pi\lambda k_B T$, and modified the electronic DOS by the convolution

$$N_{\mathrm{ep}}(E) = N_G(E) * \mathcal{L}(2\Gamma = 2\pi\lambda k_B T). \tag{17}$$

The chemical potential changes with temperature to conserve electrons. The adiabatic EPI contribution to the change in the electronic entropy is

$$\Delta S^{\mathrm{ad}}_{\mathrm{el,ep}} = S_{\mathrm{el}}(N_{\mathrm{ep}}) - S_{\mathrm{el}}(N_{\mathrm{G}}). \tag{18}$$

As temperature increases, the thermal excitation of d-band electrons shift the chemical potential to higher energies and away from the peak in the electronic DOS, reducing the contribution of the d-band electrons to the electron-phonon coupling strength. Hence λ should decrease at higher temperatures. To correct for this, we calculated electronic band structures for an ensemble of supercells with atom displacements appropriate for a few high temperatures, and used their electronic structures to obtain accurate values of $\Delta S^{\mathrm{ad}}_{\mathrm{el,ep}}$. These points were used to rescale the adiabatic EPI obtained from Eq. (18) as shown in Fig. 8.

More specifically, we prepared ensembles of ten supercells with atoms displaced with a Monte Carlo algorithm [46] for phonons calculated with experimental force constants [29,47,48]. For each configuration of displaced atoms, the electronic DOS (N_{MC}) was calculated, and an $\Delta S^{\mathrm{ad}}_{\mathrm{el,ep}}$ was calculated as

$$\Delta S^{\mathrm{ad}}_{\mathrm{el,ep}} = S_{\mathrm{el}}(N_{\mathrm{MC}}) - S_{\mathrm{el,G}} - \Delta S_{\mathrm{el,D}}. \tag{19}$$

These ten values of the adiabatic EPI were averaged and used to rescale the curves of $\Delta S^{\mathrm{ad}}_{\mathrm{el,ep}}(\lambda)$ from Eq. (18) at the temperatures of the calculations, (673, 853) K for Pd and (300, 900) K for Pt. This gave our preferred curves of $\Delta S^{\mathrm{ad}}_{\mathrm{el,ep}}(\mathrm{MC})$ in Fig. 8.

The entropy of Pd and Pt is mainly from phonons, which can be accounted for by the harmonic approximation. Other contributions provide about 10% of the total entropy, but this 1 k_{B}/atom at high temperatures is important thermodynamically. The contribution from the anharmonic phonons $\Delta S_{\mathrm{ph,Anh}}$ is negative at all temperatures in Pt, but in Pd it changes with temperature from positive to negative. This trend is consistent with the report from Wallace [42], but our crossover temperature is somewhat higher (at 1100 K versus 800 K). The small magnitude of $\Delta S_{\mathrm{ph,Anh}}$ could be consistent with large phonon lifetime broadening if the cubic and quartic contributions to the anharmonicity have opposing signs. Overall, the relationship

$$S_{\mathrm{ph,H}} \gg \Delta S_{\mathrm{ph,QH}} > \Delta S_{\mathrm{ph,Anh}} \tag{20}$$

holds for both Pd and Pt.

For Pd and Pt, the dilation contribution to the electron entropy $S_{\mathrm{el,D}}$ is always positive, while that from the adiabatic EPI is negative. The broadening of the electron DOS from the adiabatic EPI has a more significant influence on the electronic entropy than the dilation from thermal expansion. This differs from Al [23] or V [49], since the Fermi level in Pd or Pt is at a peak in the density of d-electron states. With lattice dilation, the chemical potential remains pinned at the top of the sharp peak. Alternatively, the EPI-induced thermal broadening moves the chemical potential to a higher energy and away from the peak, giving a stronger temperature dependence to $\Delta S^{\mathrm{ad}}_{\mathrm{el,ep}}$. Examples of these effects are shown in Fig. 9 for Pt.

We considered, but neglected, the configurational entropy of thermal vacancies, since it is quite small $S_{\mathrm{vac}} < 1.8 \times 10^{-3}\ k_{\mathrm{B}}/\mathrm{atom}$ (assuming a vacancy formation energy [50] $E_{\mathrm{vac}} > 1.15\,\mathrm{eV}$). We also neglected $\Delta S^{\mathrm{na}}_{\mathrm{ep}}$, expecting it to be small, especially at high temperatures. Finally, entropic contributions from paramagnons [51] are possible in Pd, but the final discrepancies of total entropies are similarly small for both Pt and Pd, so such a contribution is likely to be small for Pd.

Figures 8(a) and 8(c) compare the total entropy from our measured phonon DOS and DFT calculations ($S_{\mathrm{ph}} + S_{\mathrm{el}} + \Delta S^{\mathrm{ad}}_{\mathrm{el,ep}}$) with calorimetry results reported by Arblaster [44,45]. The agreement is excellent.

V. CONCLUSIONS

An experimental and computational study was performed on the lattice dynamics and statistical mechanics of palladium and platinum from 7 K to 1576 K. Phonon densities of states, measured by inelastic neutron scattering experiments, softened and broadened with temperature. Calculations showed that electron-phonon scattering is the dominant mechanism for the phonon lifetime broadening at low temperatures, whereas phonon-phonon scattering dominates at high temperatures.

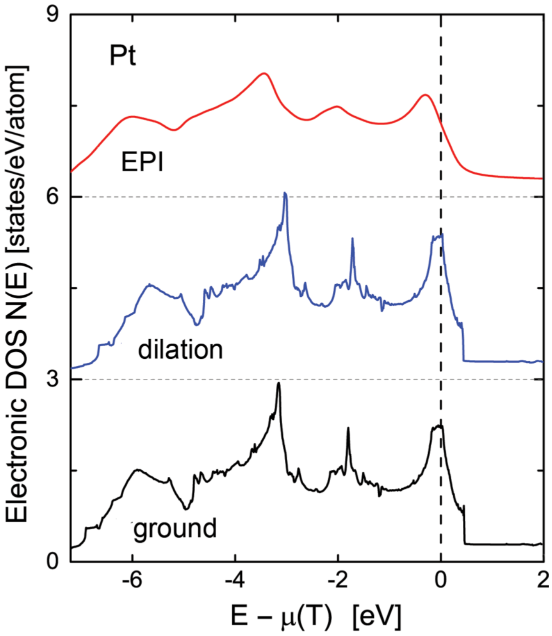

FIG. 9. The electronic DOS of Pt at the ground state, with dilation at 976 K, and with thermal broadening by the adiabatic electron-phonon interaction at 976 K. Curves are offset for clarity.

The peaks in the phonon DOS from longitudinal and transverse phonons showed distinctly different thermal broadenings. The requirement for a population of thermal phonons for upscattering suppressed the characteristic lifetime broadening of transverse phonons until the temperature exceeded 500 or 600 K, whereas the characteristic broadening of longitudinal phonons was approximately linear with temperature.

The individual components to the total entropy of palladium and platinum were assessed. The dilation from thermal expansion makes positive contributions to the entropy from both phonons or electrons. For phonons, the contribution from thermal expansion (quasiharmonicity) is larger than that from the anharmonicity. In Pt, the anharmonic contribution to phonon entropy is negative, whereas in Pd it is positive at low temperature and becomes negative above approximately 1100 K. For electrons, the effect of the adiabatic electron-phonon interaction (EPI) is negative for both Pd and Pt. For electrons, the adiabatic EPI has a larger effect on the entropy than the effect of thermal expansion. At $T = 0$ K, the Fermi level is at a sharp peak of DOS from the d band, making the electronic entropy more sensitive to thermal effects on the adiabatic EPI. With measured phonon densities of states, and with calculations of the important electronic contributions to the entropy, statistical mechanics gave total entropies of Pd and Pt metal in excellent agreement with entropies from classical thermodynamics based on heat capacity measurements.

ACKNOWLEDGMENTS

This work was supported by the Department of Energy through the Office of Basic Energy Sciences Grant No. DE-FG02-03ER46055, and benefited from DANSE software developed under NSF Grant No. DMR-0520547. A portion of this research used resources at the Spallation Neutron Source, a DOE Office of Science User Facility operated by the Oak Ridge National Laboratory. C.W.L.'s work is supported by Energy Frontier Research in Extreme Environments (EFree) Center, an Energy Frontier Research Center funded by the U.S. Department of Energy, Office of Science under Award No. DESC0001057.

Y.S. and C.W.L. contributed equally to this work.

---

[1] G. Grimvall, *The Electron-Phonon interaction in metals* (North-Holland, Amsterdam, 1981).
[2] D. C. Wallace, *Statistical physics of crystals and liquids: a guide to highly accurate equations of state* (World Scientific, Singapore, 2002).
[3] D. C. Wallace, *Thermodynamics of crystals* (Dover, New York, 1998).
[4] N. Bock, D. Coffey, and D. C. Wallace, Nonadiabatic contributions to the free energy from the electron-phonon interaction in Na, K, Al, and Pb, Phys. Rev. B **72**, 155120 (2005).
[5] X. Tang, C. W. Li, and B. Fultz, Anharmonicity-induced phonon broadening in aluminum at high temperatures, Phys. Rev. B **82**, 184301 (2010).
[6] X. Tang and B. Fultz, First-principles study of phonon linewidths in noble metals, Phys. Rev. B **84**, 054303 (2011).
[7] K. M. Ho, M. L. Cohen, and W. E. Pickett, Maximum Superconducting Transition Temperatures in A15 Compounds?, Phys. Rev. Lett. **41**, 815 (1978).
[8] B. N. Harmon and S. K. Sinha, Electron-phonon spectral function and mass enhancement of niobium, Phys. Rev. B **16**, 3919 (1977).
[9] P. B. Allen and J. C. K. Hui, Thermodynamics of solids: Corrections from electron-phonon interactions, Z. Phys. B **37**, 33 (1980).
[10] S. M. Shapiro, G. Shirane, and J. D. Axe, Measurements of the electron-phonon interaction in Nb by inelastic neutron scattering, Phys. Rev. B **12**, 4899 (1975).
[11] N. Suzuki and M. Otani, Theoretical study on the lattice dynamics and electronphonon interaction of vanadium under high pressures, J. Phys. Condens. Matter **14**, 10869 (2002).
[12] O. Delaire, M. S. Lucas, J. A. Muñoz, M. Kresch, and B. Fultz, Adiabatic Electron-Phonon Interaction and High-Temperature Thermodynamics of A15 Compounds, Phys. Rev. Lett. **101**, 105504 (2008).
[13] J. A. Muñoz, M. S. Lucas, O. Delaire, M. L. Winterrose, L. Mauger, C. W. Li, A. O. Sheets, M. B. Stone, D. L. Abernathy, Y. Xiao, P. Chow, and B. Fultz, Positive Vibrational Entropy of Chemical Ordering in FeV, Phys. Rev. Lett. **107**, 115501 (2011).
[14] O. Delaire, K. Marty, M. B. Stone, P. R. C. Kent, M. S. Lucas, D. L. Abernathy, D. Mandrus, and B. C. Sales, Phonon softening and metallization of a narrow-gap semiconductor by thermal disorder, Proc. Natl. Acad. Sci. USA **108**, 4725 (2011).
[15] P. B. Allen, Anharmonic phonon quasiparticle theory of zero-point and thermal shifts in insulators: Heat capacity, bulk modulus, and thermal expansion, Phys. Rev. B **92**, 064106 (2015).
[16] A. A. Maradudin and A. E. Fein, Scattering of neutrons by an anharmonic crystal, Phys. Rev. **128**, 2589 (1962).

[17] R. A. Cowley, Anharmonic crystals, Rep. Prog. Phys. **31**, 123 (1968).
[18] L. D. Lloyd, R. L. Johnston, S. Salhi, and N. T. Wilson, Theoretical investigation of isomer stability in platinum–palladium nanoalloy clusters, J. Mater. Chem. **14**, 1691 (2004).
[19] A. Cowley and B. Woodward, A healthy future: Platinum in medical applications, Platinum Metals Review **55**, 98 (2011).
[20] R. Gaita and S. J. Al-Bazi, An ion-exchange method for selective separation of palladium, platinum and rhodium from solutions obtained by leaching automotive catalytic converters, Talanta **42**, 249 (1995).
[21] I. Y. Sklyadneva, A. Leonardo, P. M. Echenique, S. V. Eremeev, and E. V. Chulkov, Electronphonon contribution to the phonon and excited electron (hole) linewidths in bulk pd, J. Phys. Condens. Matter **18**, 7923 (2006).
[22] DRCS, http://danse.us/trac/DrChops.
[23] M. Kresch, M. Lucas, O. Delaire, J. Y. Y. Lin, and B. Fultz, Phonons in aluminum at high temperatures studied by inelastic neutron scattering, Phys. Rev. B **77**, 024301 (2008).
[24] G. Kresse and J. Furthmüller, Efficiency of ab-initio total energy calculations for metals and semiconductors using a plane-wave basis set, Comput. Mater. Sci. **6**, 15 (1996).
[25] G. Kresse and J. Furthmüller, *Ab initio* molecular dynamics for liquid metals, Phys. Rev. B **47**, 558 (1993).
[26] G. Kresse and J. Furthmüller, Efficient iterative schemes for *ab initio* total-energy calculations using a plane-wave basis set, Phys. Rev. B **54**, 11169 (1996).
[27] S. Baroni, S. de Gironcoli, A. Dal Corso, and P. Giannozzi, http://www.pwscf.org.
[28] A. P. Miiller and B. N. Brockhouse, Anomalous Behavior of the Lattice Vibrations and the Electronic Specific Heat of Palladium, Phys. Rev. Lett. **20**, 798 (1968).
[29] D. H. Dutton, B. N. Brockhouse, and A. P. Miiller, Crystal dynamics of platinum by inelastic neutron scattering, Can. J. Phys. **50**, 2915 (1972).
[30] A. P. Miiller, Real and virtual Kohn effect in palladium by inelastic neutron scattering, Can. J. Phys. **53**, 2491 (1975).
[31] M. Palumbo, B. Burton, A. Costa e Silva, B. Fultz, B. Grabowski, G. Grimvall, B. Hallstedt, O. Hellman, B. Lindahl, A. Schneider, P. E. A. Turchi, and W. Xiong, Thermodynamic modeling of crystalline unary phases, Phys. Status Solidi B **251**, 14 (2014).
[32] M. Wierzbowska, S. de Gironcoli, and P. Giannozzi, arXiv:cond-mat/0504077.
[33] P. B. Allen, Empirical electron-phonon λ values from resistivity of cubic metallic elements, Phys. Rev. B **36**, 2920 (1987).
[34] B. Fultz, Vibrational thermodynamics of materials, Prog. Mater. Sci. **55**, 247 (2010).
[35] Y. Fei, J. Li, K. Hirose, W. Minarik, J. van Orman, C. Sanloup, W. van Westrenen, T. Komabayashi, and K. Funakoshi, A critical evaluation of pressure scales at high temperatures by in situ x-ray diffraction measurements, Phys. Earth Planet. Inter. **143-144**, 515 (2004).
[36] S. Ono, J. P. Brodholt, and G. D. Price, Elastic, thermal and structural properties of platinum, J. Phys. Chem. Solids **72**, 169 (2011).
[37] P. I. Dorogokupets and A. Dewaele, Equations of state of MgO, Au, Pt, NaCl-B1, and NaCl-B2: Internally consistent high-temperature pressure scales, High Press. Res. **27**, 431 (2007).
[38] M. Yoshihara, R. B. McLellan, and F. R. Brotzen, The high-temperature elastic properties of palladium single crystals, Acta Metall. **35**, 775 (1987).
[39] S. M. Collard and R. B. McLellan, High-temperature elastic constants of platinum single crystals, Acta Metall. Mater. **40**, 699 (1992).
[40] J. W. Arblaster, The thermodynamic properties of platinum, Platinum Metals Review **49**, 141 (2005).
[41] J. W. Arblaster, Crystallographic properties of palladium, Platinum Metals Review **56**, 181 (2012).
[42] O. Eriksson, J. M. Wills, and D. Wallace, Electronic, quasi-harmonic, and anharmonic entropies of transition metals, Phys. Rev. B **46**, 5221 (1992).
[43] M. Thiessen, Corrections to the electronic heat capacity of metals due to finite lifetimes of the conduction electrons, Int. J. Thermophys. **7**, 1183 (1986).
[44] J. W. Arblaster, The thermodynamic properties of palladium on ITS-90, Calphad **19**, 327 (1995).
[45] J. W. Arblaster, Thermodynamic properties of the platinum metals on ITS-90, Platinum Metals Review(UK) **40**, 62 (1996).
[46] P. Steneteg, O. Hellman, O. Y. Vekilova, N. Shulumba, F. Tasnádi, and I. A. Abrikosov, Temperature dependence of tin elastic constants from *ab initio* molecular dynamics simulations, Phys. Rev. B **87**, 094114 (2013).
[47] A. P. Miiller and B. N. Brockhouse, Crystal dynamics and electronic specific heats of palladium and copper, Can. J. Phys. **49**, 704 (1971).
[48] R. Ohrlich and W. Drexel, Lattice dynamics of platinum, in *Neutron Inelastic Scattering Vol. I. Proceedings of a Symposium on Neutron Inelastic Scattering* (International Atomic Energy Agency, Vienna, 1968).
[49] O. Delaire, M. Kresch, J. A. Muñoz, M. S. Lucas, J. Y. Y. Lin, and B. Fultz, Electron-phonon interactions and high-temperature thermodynamics of vanadium and its alloys, Phys. Rev. B **77**, 214112 (2008).
[50] T. R. Mattsson and A. E. Mattsson, Calculating the vacancy formation energy in metals: Pt, Pd, and Mo, Phys. Rev. B **66**, 214110 (2002).
[51] R. Doubble, S. M. Hayden, P. Dai, H. A. Mook, J. R. Thompson, and C. D. Frost, Direct Observation of Paramagnons in Palladium, Phys. Rev. Lett. **105**, 027207 (2010).